J. Ocean Univ. China (Oceanic and Coastal Sea Research)
https://doi.org/10.1007/s11802-018-3443-8
ISSN 1672-5182, 2018 17 (1): 156-168
http://www.ouc.edu.cn/xbywb/
E-mail:xbywb@ouc.edu.cn

Seismotectonics of the Taiwan Shoal Region in the Northeastern South China Sea: Insights from the Crustal Structure

WAN Kuiyuan[1), 2)], SUN Jinlong[1)], XU Huilong[1)], XIE Xiaoling[3)], XIA Shaohong[1),*], ZHANG Xiang[4)], CAO Jinghe[1)], ZHAO Fang[1)], and FAN Chaoyan[1), 2)]

1) *CAS Key Laboratory of Ocean and Marginal Sea Geology*, *South China Sea Institute of Oceanology*, *Chinese Academy of Sciences*, *Guangzhou* 510301, *China*
2) *University of Chinese Academy of Sciences*, *Beijing* 100049, *China*
3) *Earthquake Administration of Hainan Province*, *Haikou* 570203, *China*
4) *Earthquake Administration of Guangdong Province*, *Guangzhou* 510070, *China*

(Received February 22, 2017; revised May 16, 2017; accepted July 4, 2017)

Abstract A cluster of earthquakes occurred in the Taiwan Shoal region on the outer rise of the Manila Trench. Although most were of small to medium magnitudes, one strong earthquake occurred on September 16, 1994. Several previous studies have provided important information to progress our understanding of this single earthquake. However, little is currently known about the earthquake cluster, and it is necessary to investigate the deep crustal structure of the Taiwan Shoal region to understand the mechanisms involved in controlling and generating it. This study presents a two-dimensional seismic tomographic image of the crustal structure along the OBS2012 profile based on ocean-bottom seismograph (OBS) data, which exhibits a high-velocity anomaly flanked by low-velocity anomalies in the upper crust beneath the Taiwan Shoal. In this study, 765 earthquakes (Richter magnitude $M_L > 1.5$) occurring between 1991 and 2015 were studied and analyses of earthquake epicenters, regional faults, and the crustal structure provides an improved understanding of the nature of active tectonics in this region. Results of analyses indicate firstly that the high-velocity area represents major asperities that correspond to the location of the earthquake cluster and where stress is concentrated. It is also depicted that the earthquake cluster was influenced by fault interactions. However, the September 1994 earthquake occurred independently of these seismic activities and was associated with reactivation of a preexisting fault. It is also determined that slab pull is resisted by the exposed precollision accretionary prism, and the resistive force is causing accumulation of inplane compressive-stress. This may trigger a future damaging earthquake in the Taiwan Shoal region.

Key words earthquake cluster; crustal structure; fault interactions; outer rise; Taiwan Shoal

1 Introduction

The northeastern margin of the South China Sea (SCS) corresponds to the southeastern edge of the Eurasian tectonic plate, where seismic activity is frequent (Chen and Huang, 1984; Liu *et al*., 1994; Ren *et al*., 2002) (Fig.1). The complex tectonic movements occurring between the Eurasian plate and the Philippine Sea plate are characterized by distinctive seismicities and seismogenic mechanisms (Sun *et al*., 2012). According to their focal mechanisms, intense- and intermediate-magnitude seismic activities are characterized by strike-slip earthquakes along the coast of southern China (Lin *et al*., 2009). Seismic activity in the northeastern SCS mainly results from compressional tectonic activity. However, the Taiwan Shoal region is at the outer rise of Manila Trench where earthquakes result from normal faulting (Kao and Wu, 1996; Zheng *et al*., 1998).

Local normal-faulting events have attracted the attention of tectonic scientists and geologists for many years (*e.g.*, Burchfiel and Royden, 1985). Some studies have depicted that intraslab earthquake activity beneath the outer rise in subduction zones is characterized by shallow normal-faulting ruptures with depths of less than 30 km (*e.g.*, Christensen and Ruff, 1988; Lee and Lin, 2013). However, other studies have depicted that deeper compressional earthquakes are triggered by a slow bending of the crust when subduction zones are strongly coupled (*e.g.*, Fromm *et al*., 2006; Clouard *et al*., 2007; Todd and Lay, 2013). In addition, detailed studies of outer-rise seismicity have defined important constraints on local deformation, fracture distribution, stress changes, and interplate coupling (Chapple and Forsyth, 1979; Christensen and Ruff, 1988; Müller *et al*., 1996a, 1996b; Clouard *et al*., 2007; Todd and Lay, 2013).

The earthquake cluster occurring in the Taiwan Shoal region near the Manila Trench is distributed over an area of 60 $km^2 \times 60$ km^2 at depths ranging from 5 to 15 km (Figs.1 and 2), and concentrated in the vicinity of the faults.

* Corresponding author. E-mail: shxia@scsio.ac.cn

Intermediate-magnitude (Richter magnitude M_L = 4.0–6.0) earthquakes have been distributed from the northeast to the southwest, approximately parallel to the trench, which is in accordance with the distribution of tension stresses associated with bending of the crust in the subduction zone (Stauder, 1968a, 1968b; Chapple and Forsyth, 1979; Seno and Yamanaka, 1996). However, the September 1994 earthquake (M_L = 7.3) was caused by east–west striking normal fault planes lying approximately perpendicular to the trench (Kao and Wu, 1996; Zheng *et al*., 1998). Therefore, Zheng *et al*. (1998) suggested that this earthquake and its aftershocks were a set of events occurring independently from other seismic activity within the Taiwan Shoal region.

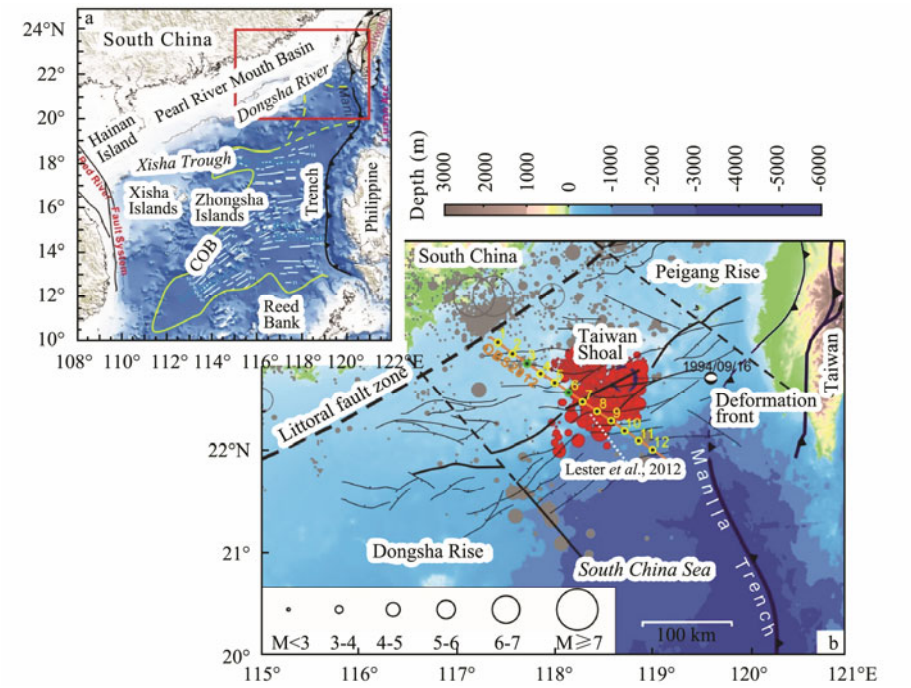

Fig.1 (a) Geological framework of the South China Sea (SCS) region. (b) Generalized map showing earthquake distribution and location of active faults in the northeastern SCS. Positions of OBSs and air gun shooting track with 835 shots are shown by OBS numbers and the brown line, respectively. Earthquake locations were obtained from databases of the China National Seismic Network and the Guangdong Seismic Network. Solid black lines indicate active faults identified on multichannel seismic profiles run between 1980 and 2010 by the Guangzhou Marine Geological Survey (Yang et al., 2015); dashed black lines represent inferred faults (Xu et al., 2006; Yang et al., 2015); white dashed line represents multichannel seismic profile obtained from Lester et al. (2012). Focal mechanism and location of September 16, 1994 earthquake (depicted in blue) were obtained from Kao and Wu (1996) and Zheng et al. (1998).

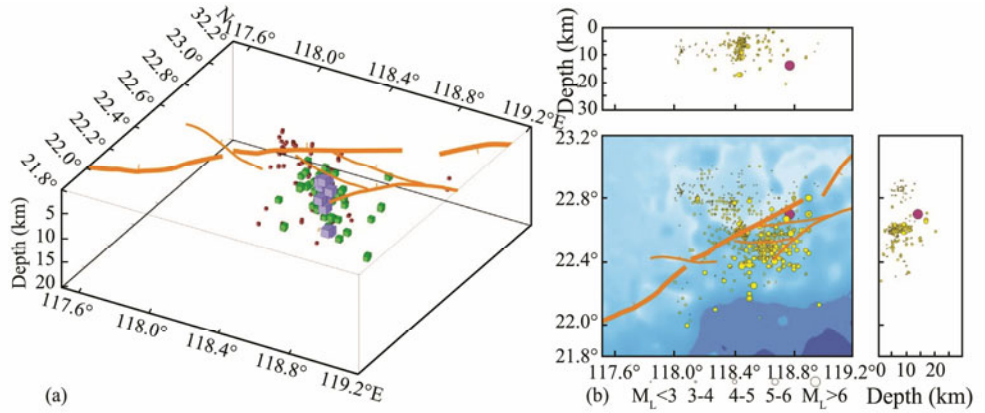

Fig.2 Earthquake locations within Taiwan Shoal selected for this study. (a) Three-dimensional distribution of earthquakes with depth: red cubes indicate a magnitude (M_L) of less than 3.0; green cubes indicate M_L4.0–5.0; and blue cubes indicate M_L5.0–6.0. (b) The hypocentral distribution of the 764 selected earthquakes, and the focal depths of the 255 earthquakes whose associated data were considered adequately accurate for inclusion in this study. The earthquake of September 16, 1994 is represented by the purple circle.

The Taiwan Shoal region is thus evidently affected by complex tectonic processes. Intermediate-magnitude seismic activity is very frequent in the region of the earthquake cluster, but limited research has been conducted on

the associated events. According to the seismic record for the region, no events higher than that of the September 1994 event have been recorded. Therefore, we propose that the rupture processes relating to the cluster and the September 1994 event are significantly different. In this study, we seek to identify seismogenic mechanisms within the crustal structure that are related to particular stress states, the earthquake cluster, and the 1994 Taiwan Shoal earthquake, with a strong emphasis on determining magnetic and gravity anomalies.

An Ocean Bottom Seismograph (OBS) wide-angle seismic survey is an effective method of imaging the deep crustal structure. For this study, we acquired imagery taken between June and July 2012 along the OBS2012 profile, which transects the Taiwan Shoal. Using this imagery, we modeled the crustal structure using the RAY-INVR velocity-modeling program. The crystal structure exhibits a high-velocity anomaly in the upper crust beneath the Taiwan Shoal and is flanked by relatively low-velocity anomalies on either side. Detailed studies of the material properties of the crust in this area enabled us to understand the nucleation and rupture processes of earthquakes (Zhao *et al*., 1996, 2002). Many previous studies have revealed that the heterogeneity of the crust plays an important role in generating earthquakes (Lees and Nicholson, 1993; Zhao *et al*., 1996, 2004; Srinagesh *et al*., 2000; Chen *et al*., 2001; Mishra and Zhao, 2003; Wang and Zhao, 2006; Xia *et al*., 2008; Wang *et al*., 2015). However, there appears to be little or no relation between the geologic structures and the occurrence of earthquakes in our study area.

In this paper, the following research questions are asked with respect to the crustal structure of the Taiwan Shoal:

1) What geophysical characteristics influence seismic activity in the Taiwan Shoal?

2) What is the relation between the earthquake cluster and the crustal structure?

3) Are future large earthquakes likely to occur in this region?

2 Tectonic Setting

The South China subplate and SCS subplate are relatively stable blocks bounded by a littoral fault zone (Fig.1) (Xu *et al*., 2006), and each displays weak internal deformation (Zhang *et al*., 2002; Zhang *et al*., 2005; Simons *et al*., 2007). The SCS subplate is an independent block that has been moving eastward at a rate of about 10 mm yr^{-1} since the cessation of seafloor spreading (Simons *et al*., 2007). However, its northern part depicts the effects of compressional stress and is constrained by the surrounding tectonic environment. For the South China subplate, the transfer of stress in a southeasterly direction is derived due to the collision between the India and Eurasia plate (Zhou *et al*., 2000), which has led to its southeastward movement at a rate of 39 mm yr^{-1} (Li *et al*., 2002). Conversely, the Philippine Sea plate is moving northwestward at a rate of 70 to 80 mm yr^{-1} (Seno, 1993; Wu *et al*., 2009).

From the Oligocene to the middle Miocene, continued rifting generated the oceanic lithosphere and opened up the SCS (Taylor and Hayes, 1983; Briais *et al*., 1993). However, the oceanic lithosphere in the SCS has been subducting eastward beneath the Philippine Sea plate since the early Miocene (Sibuet *et al*., 2004), which is overriding the Eurasian plate along the east-dipping Manila Trench between the islands of Taiwan and Luzon. From south to north, plate convergence gradually evolved from subduction of the SCS oceanic lithosphere beneath the Manila Trench and the initial collision between the Philippine Sea plate and the Eurasian plate (the Taiwan orogeny) (Huang *et al*., 2000; Ku and Hsu, 2009). Additionally, the Taiwan mountain belt was formed by the northwestward convergence of the Luzon Arc against the Eurasian plate margin (Angelier, 1986; Sibuet and Hsu, 2004; Sibuet *et al*., 2004).

Further, subduction of the SCS oceanic lithosphere beneath the Philippine Sea plate south of 21°20′N created a typical arc-trench system consisting of the Luzon Arc, Luzon Trough, Hengchun Ridge, and Manila Trench (Huang *et al*., 2000; Kao *et al*., 2000). However, the subduction zone trending to the north of 21°20′N developed from an initial (and then subsequently advanced) collision between the arc and the continental plate (Huang *et al*., 2000; Lester *et al*., 2013), which gradually connected with the deformation front in the western part of the Taiwan mountain belt (Hsu *et al*., 2004). It is considered that the differences between the tectonic behaviors may be caused by variations in the internal structures of the incoming plates (from a northerly to southerly direction) (Wu *et al*., 2009; Chen *et al*., 2014).

It has further been determined that the northeastern SCS features uplifting of abundant and discrepant fault blocks in connection with the structural framework of the Yanshanian. These faults were reactivated during the Cenozoic. During the Paleocene, the northeastern SCS developed in a back-arc extensional setting under the influence of the subduction of the paleo-Pacific plate (Zhou and Li, 2000; Li and Li, 2007; Shi and Li, 2012; Wang and Shu, 2012; Yan *et al*., 2014). In the northern to northeastern part of the Tainan Basin, a series of syngenetic master faults and abundant secondary faults developed, in an approximately east to west direction (Ding *et al*., 2004), and these eventually divided the Tainan Basin into the Northern Depression, Central Uplift, and Southern Depression (Lin *et al*., 2003; Li *et al*., 2007). Huang *et al*. (2001) believe that the Tainan Basin in the northeastern SCS experienced two further episodes of normal faulting, one occurring during the Oligocene and the other during the late Miocene. On the basis of multichannel seismic data, Li *et al*. (2007) revealed that normal faults in the Tainan Basin were continuously active until the late Cenozoic.

3 Data and Modeling

3.1 Data and Analysis

This study focuses on data obtained from two sources relating to earthquakes occurring in the Taiwan Shoal region during two time-periods, as follows: 1) 1991–2005,

recorded by the China National Seismic Network, and 2) 2006–2015, recorded by the Guangdong Seismic Network. Of the 764 earthquakes selected, 286 were of a magnitude less than M_L3.0; 356 were between M_L3.0 and 4.0; 110 between M_L4.0 and 5.0; and 12 between M_L5.0 and 6.0. These data also include the September 1994 Taiwan Shoal earthquake (M_L7.3) (Kao and Wu, 1996; Zheng *et al*., 1998), which is discussed later in this study. As the focal depths of some earthquakes could not be confirmed (because they occurred too far from recording stations and seismic signals were compromised by noise), only the focal depths of 255 of the 764 earthquakes were considered accurate enough for use in this study.

Wide-angle OBS data were acquired in the Taiwan Shoal area by the *R/V* '*Shiyan 2*' of the South China Sea Institute of Oceanology in June and July of 2012. Twelve four-component OBSs, spaced at approximately 20-km intervals, were deployed along a northwest-southeast trending profile with a length of 240-km spanning across the seismically active region (Fig.1). Data from recorded sections were filtered from 3 Hz to 15 Hz using a classical band-pass Butterworth filter to enhance the signal-to-noise (S/N) ratios of some of the weaker seismic activities. Further, a gain was applied by an offset to optimize the picking at different offset ranges. The P-wave model was calculated from vertical components of most OBS data and from hydrophone components of seismic profiles OBS05, OBS08, and OBS12 (which were of higher quality than the vertical components used in this study). We manually selected 7677 reflection and refraction arrivals: the Ps, Pg1, Pg2, and Pn phases, which denote the rays refracted in the sediment, upper crust, lower crust, and upper mantle, respectively, and the PcP and PmP phases that indicate reflections from the Conrad and crust-mantle boundary (Moho), respectively. Among these data, 7496 were used for travel-time fitting. Seismic record sections were plotted for each OBS with a reduced velocity of 6.0 km s^{-1} and having a 3–12 Hz band-pass filter (Figs.3, 4).

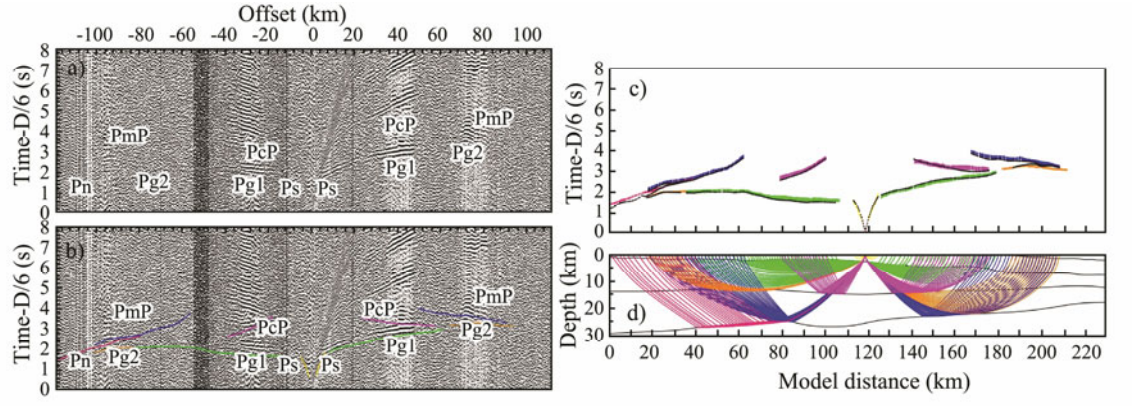

Fig.3 a) Seismic profile of station OBS07 at a reduction velocity of 6 km s^{-1} and a bandpass filter of 3–12 Hz; b) pick-up of seismic phase at station OBS07; c) matching between observed arrival time and calculated arrival time; d) P-wave velocity model and ray-tracing at station OBS07.

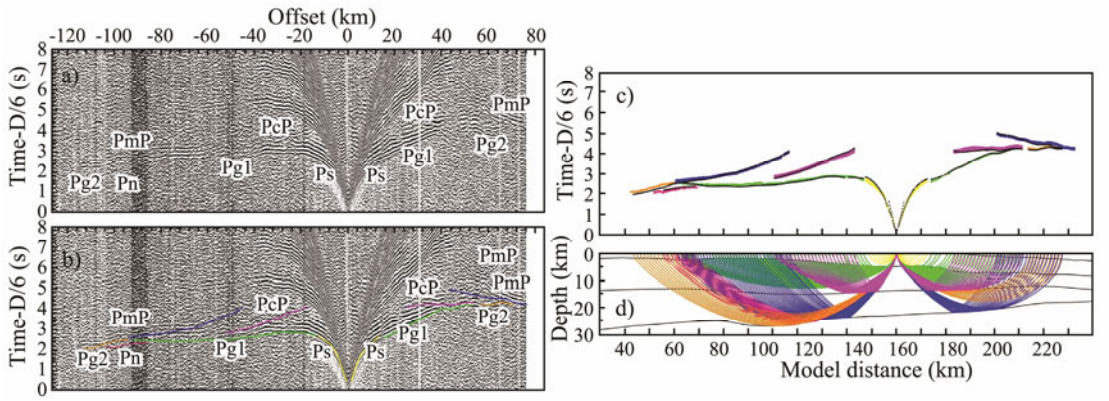

Fig.4. a) Seismic profile of station OBS09 at a reduction velocity of 6 km s^{-1} and bandpass filter of 3–12 Hz; b) pick-up of seismic phase at station OBS09; c) matching between observed arrival time and calculated arrival time; d) P-wave velocity model and ray-tracing of station OBS09.

3.2 Modeling Procedure

A simple model was constructed using previous seismic activity and seismic reflection/refraction sections (*e.g.*, Wang *et al*., 2006; Li *et al*., 2007; Lester *et al*., 2012, 2014). Secondary Pg phases are useful indicators of sediment thickness (Wan *et al*., 2016). Therefore, the P-wave velocities within shallow sedimentary layers were accurately calculated by applying secondary Pg phases. The velocity model was derived from the refracted and

reflected arrivals recorded by the OBS profiles and was mainly constructed using manual trial and error until the modeled travel times were consistent with observed travel times (Zelt and Smith, 1992). Depending on the S/N ratios, uncertainties ranging from 0.02 to 0.10 s were assigned. The formal error analysis of all OBS profiles and calculation error analyses of the individual phases are summarized in Tables 1 and 2, respectively. The χ^2 value of forward modeling was determined as 1.688, and the total root-mean-square travel-time residual was found to be 0.081 s (Wan *et al*., 2017). The coverage of the ray paths exceeded 20 hits, and reached 30 to 40 hits among OBS profiles and over 60 hits in the upper crust (Fig.5).

In this study, the earthquake cluster was mainly analyzed using the RAYINVR modeling program. The RAYINVR's *F*-test program was used to estimate the velocity and depth uncertainty of the final velocity model. For this, we slightly altered the depths and velocities until the new model fitted the observed data, and used an F-test to compare the χ^2 values of the two final models to ensure the models only differed by a 5% significance level (Zelt and Smith, 1992). The resulting final model depicts uncertainties of −0.2–0.1 km s^{-1} for velocities in the upper crust and −0.2–0.5 km for the Moho depth (Fig.6).

Table 1 Numbers of picks, RMS misfit and χ^2 values for individual OBS station, using forward modeling

OBS stations	Components	Depth (m)	No. of picks	RMS(S)	χ^2
OBS01	Vertical	44	475	0.083	1.629
OBS02	Vertical	30	499	0.048	1.287
OBS04	Vertical	28	560	0.092	2.184
OBS05	Hydrophone	30	946	0.074	2.199
OBS07	Vertical	39	1049	0.090	1.662
OBS08	Hydrophone	72	973	0.051	1.119
OBS09	Vertical	107	1324	0.077	1.364
OBS10	Vertical	143	728	0.094	2.050
OBS11	Vertical	1000	560	0.069	1.405
OBS12	Hydrophone	1300	401	0.085	2.664

Table 2 RMS misfit and χ^2 values for individual seismic phases in forward modeling

Phase	Name	No. of picks	Uncertainty of picks (s)	RMS(S)	χ^2
Direct wave		176	0.020–0.030	0.047	2.505
Sediment refraction	Ps	473	0.050	0.092	1.855
Refraction in upper crust	Pg1	2836	0.050	0.078	2.047
Refraction in lower crust	Pg2	692	0.080	0.068	0.718
Reflection at the Conrad	PcP	649	0.080	0.109	1.499
Reflection at the Moho	PmP	2128	0.080–0.100	0.081	1.128
Refraction in upper mantle	Pn	588	0.080–0.100	0.070	0.984
All seismic phases				0.081	1.688

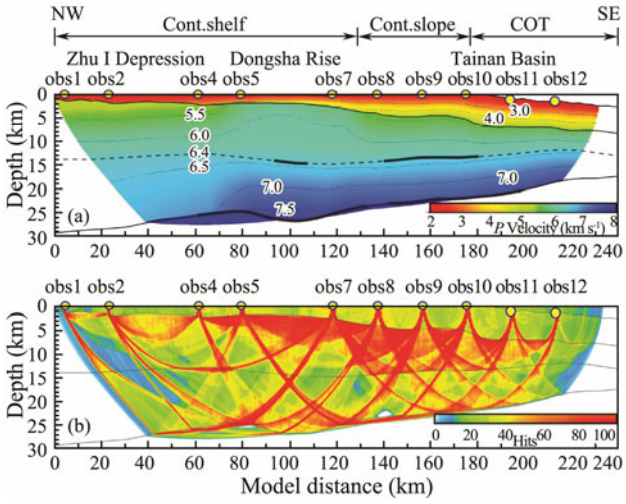

Fig.5 (a) Results of forward-velocity RAYINVR model. Yellow circles represent OBSs locations along OBS2012 profile; thick black lines indicate locations where the Conrad interface is constrained by PcP arrivals and where the Moho interface is constrained by PmP arrivals. (b) Ray coverage density throughout the model. White areas are unconstrained by ray tracing; ray coverage improves from green to red.

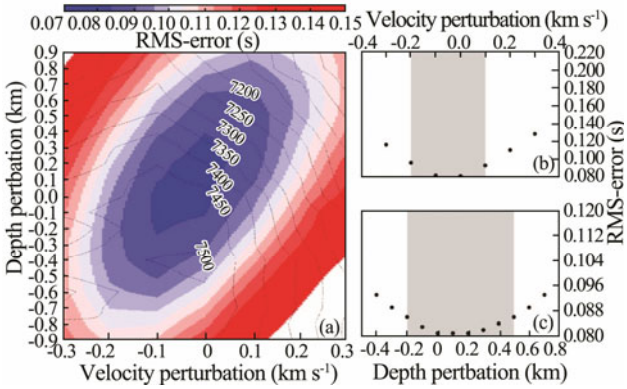

Fig.6 Error analysis by model perturbation. (a) Results from simultaneously varying Moho depth and velocities in lower crustal layer; contours represent number of picks explained by forward model. (b) Results from only varying velocities in lower crust. (c) Results from varying the Moho depth. Gray box represents uncertainties determined in the most important boundaries calculated from 95% confidence limit of *F*-test.

A model with a good spatial resolution provides the best accuracy. Therefore, an estimate of the spatial resolution of the final model was obtained using the checker-

board test (Zhao *et al*., 1992). For this, we firstly created a synthetic velocity model with: 1) equal distances of 20 km in landscape in the range of 0–40 km and 180–240 km of the model; and 2) equal distances of 10 km in the range of 40–160 km (Fig.7a). Further, we added velocity- perturbed values (±0.2 km s^{-1}) that were equal in magnitude but opposite in sign at adjacent nodes. Interfaces of the RAYINVR model were then applied in the vertical direction and the inversion result is depicted in Fig.7b. The velocity perturbation patterns are well-recovered across most of the model, but not so well-recovered at either end. This indicates that the resolution used in the middle parts of the structure is better than that for the 20-km-wide swath in the lateral.

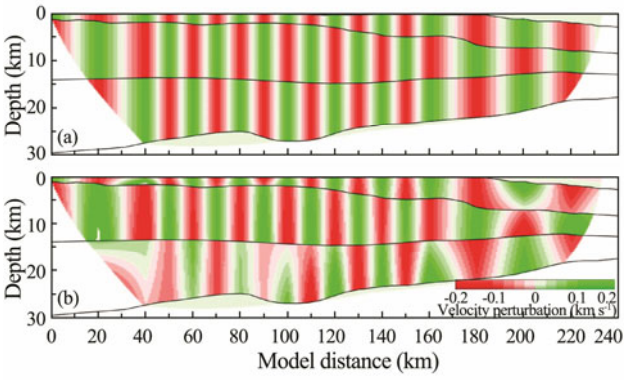

Fig.7 (a) Synthetic velocity perturbation using checkerboard test. (b) Calculated velocity perturbation for checkerboard test.

4 Crustal Structure

Fig.5 illustrates the P-wave velocity structure model along the wide-angle OBS profile across the ruptured zone of the September 1994 Taiwan Shoal earthquake. In this section, we discuss the use of our model with respect to focusing on the probable seismogenic structure from the Tainan Basin toward the Taiwan Shoal. Our model is divided into three sections along a distance of 240 km as follows: the Zhu I Depression from 0 to 70 km, the Taiwan Shoal region from 70 to 130 km, and the Tainan Basin from 130 to 240 km. The model includes five layers, and their respective velocity categories as follows: water, sediment, upper crust, lower crust, and upper mantle (Fig.5). The velocity structure indicates thickening in the sediment layer from the Taiwan Shoal to the Tainan Basin, where the maximum thickness is about 6.0 km. There are evident increases in the velocities through the sediment layer in the Tainan Basin, which vary from 1.8 km s^{-1} near the top to 5.3 km s^{-1} at the base. However, the crustal layers gradually thin seaward; the upper crust thins from 13 to 4 km and the lower crust from 15 to 6 km. The model also reveals the existence of: 1) a thick high-velocity layer in the lower crust extending from the continental shelf to the continent–ocean transition zone; and 2) a high- velocity layer in the upper crust beneath the Taiwan Shoal. Lateral variations in velocities indicate that the crust is comprised of heterogeneous materials.

4.1 Continental Shelf from Zhu I Depression Region Through Taiwan Shoal Region

The crustal structure along the profile from the Zhu I Depression to the Taiwan Shoal (from 0 to 130 km) is characterized by a thin (1–3 km) sedimentary layer and a thick (21–27 km) crystalline crust. The sedimentary layer has velocities varying from 1.8 km s^{-1} near the top to 4.0 km s^{-1} at the base. Beneath this layer, the thick crystalline crust has velocities ranging from 5.0–6.4 km s^{-1} in its upper part to 6.4–7.6 km s^{-1} in the lower part. The crust thins seaward, whereas the Taiwan Shoal exhibits a slight local thickening accompanying the increase in the Moho depth. The velocity (5.5–6.4 km s^{-1}) in the upper crust across the Taiwan Shoal is greater than that in the upper crust across the Zhu I Depression. The Taiwan Shoal was most likely created by volcanism and intrusion into the upper crustal section, which may be interpreted as the arc crust. With its high topography and thickened crust, the Taiwan Shoal is a striking area in the southwestern Taiwan seismic zone, where earthquakes have occurred at a high frequency.

4.2 Tainan Basin Crust

The crustal structure across the Tainan Basin (from 130 to 240 km) consists of a thick (3–7 km) sedimentary layer overlying a thin (10–21 km) crystalline crust. The sediment becomes thicker seaward and reaches its maximum thickness in the Tainan Basin. At the bottom of the sedimentary layer in the Tainan Basin, velocities reach a peak of 5.3 km s^{-1}, which is much greater than the velocities of the sedimentary layer underlying the Zhu I Depression and the Taiwan Shoal. From top to bottom, the sedimentary package in the Tainan Basin is subdivided into two major depositional sequences: the Cenozoic sequence and the Mesozoic sequence (Li *et al*., 2007; Lester *et al*., 2014). Velocities of the upper and lower crusts range from 5.5 to 6.4 km s^{-1} and from 6.4 to 7.5 km s^{-1}, respectively. The velocities of the upper crust are associated with normal continental upper crust but are lower than those for the upper crust in the Taiwan Shoal. However, velocities of 7.0 to 7.5 km s^{-1} in the lower crust are considered to be high relative to typical lower continental crustal material.

5 Discussion

5.1 Geophysical Characteristics

With reference to the elasticity theory of deformation, far-field stress may be concentrated if different elastic moduli are more heterogeneous than the surrounding area (*e.g.*, Saada, 1983). Relationships between crustal heterogeneities and large crustal earthquakes have been investigated in areas such as the Koyna seismic zone in India (Srinagesh *et al*., 2000), Niigata area of Japan (Xia *et al*., 2008), and the Lushan area of China (Wang *et al*., 2015), and these studies have concluded that high-velocity areas, or boundaries existing between high- and low-velocity anomalies may define an asperity where stress is concentrated and where large earthquakes may occur.

Fig.5 depicts that there is a high-velocity anomaly in the upper and lower crusts beneath the Taiwan Shoal and that this area is flanked by low-velocity anomalies on both sides. The high-velocity zone in the upper and lower crusts across the Taiwan Shoal is associated with an arc caused by subduction of the paleo-Pacific plate during the Mesozoic, and the seismicity is highly consistent with the presence of a high-velocity body. Consequently, we believe that the high- and low-velocity anomalies within our study area affect and control the rupturing events and may also account for gravity and magnetic anomalies.

Previous gravity and magnetic studies have provided valuable insights into the geologic framework of the northern SCS (*e.g.*, Xia *et al*., 1994; Cheng, 2004; Zhou *et al*., 2006; Li *et al*., 2008). Gravity and magnetic anomalies together define distinctive structures, some of which appear to be closely related to earthquake occurrence. Studies that indicate a correlation between gravity and magnetic anomalies and seismotectonics have been conducted in areas such as the northern Mississippi Embayment, north of Memphis, Tennessee (Hildenbrand, 1985; Hildenbrand *et al*., 2001). Hinze and Hildenbrand (1988) concluded that by providing definitions and characterizations of the following, all of which can correlate with seismicity patterns, gravity and magnetic data can be used to contribute to estimates of crustal strength: 1) regions of possible weakness (faults, sutures, and rifts), 2) areas of possible stress concentration (edges of intrusions or bends in fault zones), and 3) structural grain.

High magnetic and gravity anomalies trend southwest to northeast in the northeastern SCS (Fig.8). However, the belt with a high magnetic anomaly appears to shift northward, forming a turning point (Fig.8a). In addition, the belt with a high gravity anomaly is forked, leading to a relatively local low-gravity region within the Taiwan Shoal area (Fig.8b).

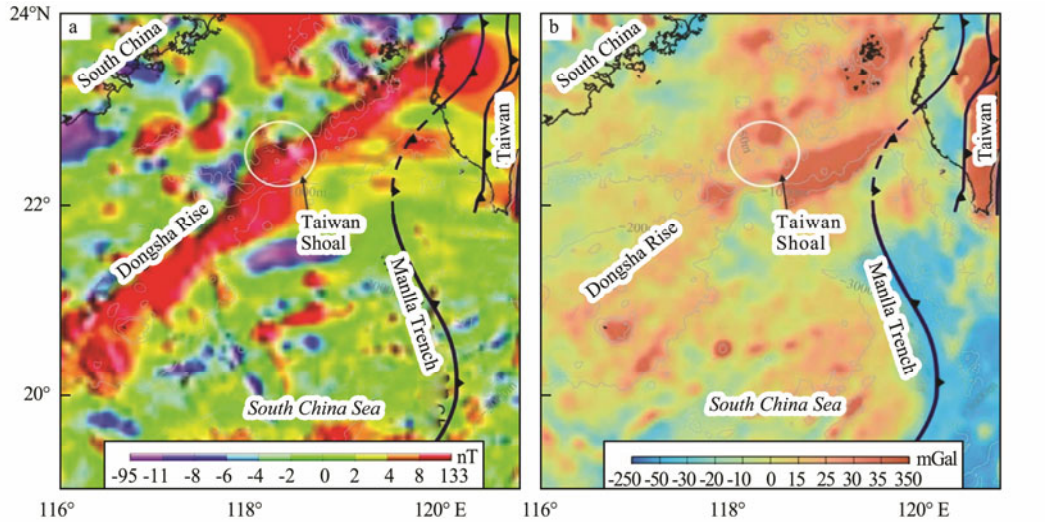

Fig.8 (a) Magnetic anomaly in the northeastern part of the South China Sea (SCS) and (b) free-air gravity anomaly in the same regions.

The earthquake cluster within this region appears to correlate spatially with this turning point and bifurcation. Coincidentally, the New Madrid seismic zone in the central United States is defined by an intersection of graben, is characterized by low gravity, and has been interpreted as a rift (Guinnsee *et al*., 1982).

Free-air gravity anomalies have been widely used to infer the state of isostatic compensation in regions (Woolard, 1959). In the case of complete equilibrium, a zero value indicates that an excess topographic load will be balanced by a low-density compensating mass (Woolard, 1959; Turcotte and Schubert, 2001). However, a high-velocity intrusive mass underlying elevated topography (such as in the Taiwan Shoal region) corresponds to a relatively low free-air gravity anomaly. This relation indicates that the low free-air gravity anomaly is caused by faults that have very large slip amplitudes and which may offset the positive mass. Furthermore, the large slip amplitude is probably responsible for the shift of the belt that exhibits a high magnetic anomaly.

5.2 Earthquake Cluster and September 16, 1994, Taiwan Shoal Earthquake

Detailed studies of the earthquake distribution and tectonic features of outer rises have defined significant constraints on stress changes, local deformation, and interplate coupling (Chapple and Forsyth, 1979; Christensen and Ruff, 1988; Clouard *et al*., 2007; Lay *et al*., 2010; Todd and Lay, 2013). Additionally, seismic activity beneath the outer rise in subduction zones has been characterized by shallow normal-faulting ruptures at depths of less than 30 km or less frequently by deeper megathrust earthquakes (*e.g.*, Christensen and Ruff, 1988). Normal faulting on outer rises has been attributed to plate-bending stresses acting on the lithosphere as the slab deforms on its approach to the trench (*e.g.*, Stauder, 1968b). Fig.1 depicts that frequent intraslab earthquakes have occurred in the Taiwan Shoal region. With the exception of the September 1994 event, most of these were of intermediate and small magnitudes. The seismicity in this area indicate

an earthquake cluster, which is mainly located at depths of 3 to 15 km and coincides with the high-velocity area in the upper crust (Fig.10).

Lees and Malin (1990) suggested that a high-velocity area can be defined by a major asperity where stress is concentrated. Except for the Manila Trench, the area of the Taiwan Shoal region characterized by high topography experienced plate bending, which precipitated the arc-continent collision in Taiwan. High-velocity areas are therefore vulnerable to faulting, and the high concentration of earthquakes in this region does indeed coincide with a high-velocity area (the area where the crust was bent sufficiently to rupture). In previous studies, Lester *et al*. (2012) proposed a continental crust plate model for the area near the Taiwan Shoal (Figs.1 and 9) that was based on multichannel seismic-reflection data and numerical calculations. This model illustrates a large number of high-angle normal faults were produced near the hinge (Fig.9). Indeed, landward-dipping listric faults are usually located below the top of a bending point (*e.g.*, Stauder, 1968b; Clouard *et al*., 2007) and their strikes are almost parallel to the trend of the trench. However, most faults in this area do not extend up to the surface except for the outcropping fault (F1) (Fig.10), which indicates that the rupture mainly occurred at depths of 3 to 13 km, where the rigid body is located.

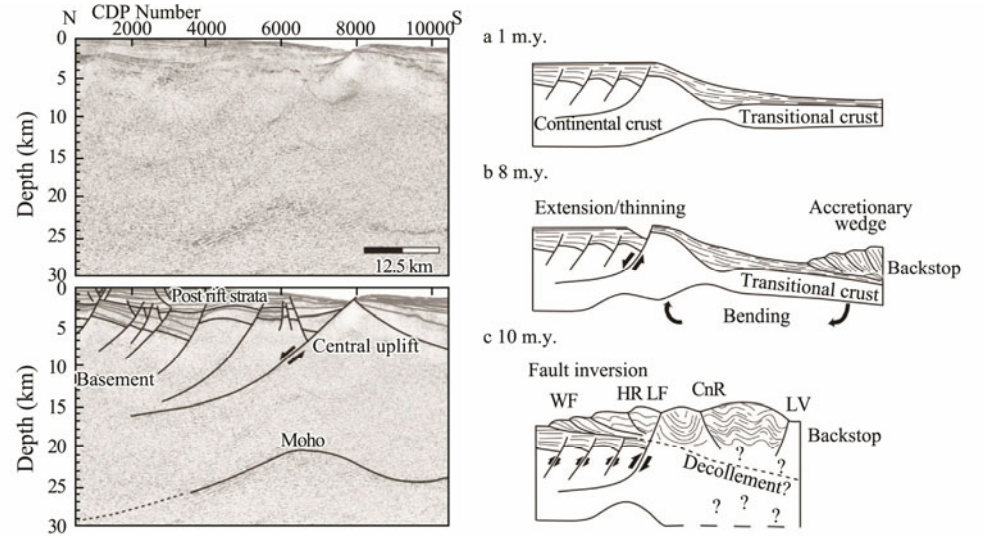

Fig.9 Depth-migrated seismic line MGL0905_07: (left) several faults are imaged, including a rift basin-bounding fault along the central uplift, which creates significant fault scarp at seafloor, thereby indicating recent activity; (right) evolutionary model of rifting at plate margins during collision (Lester *et al*., 2012). Abbreviations: western foothills fold-and-thrust belt (WF), hsuehshan range (HR), central range (CnR), and coastal range (CR). The hsuehshan range and central range are separated by the Lishan fault (LF), a major structural and morphologic boundary, and the longitudinal valley (LV) is an Eurasia-Philippine Sea plate suture.

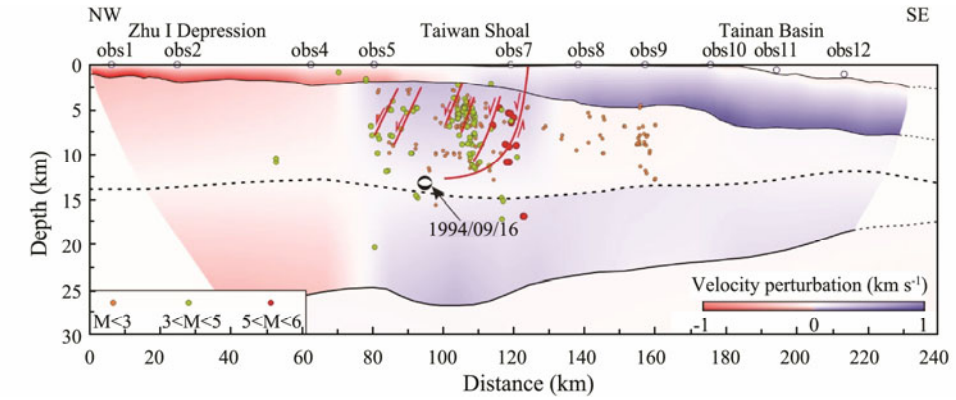

Fig.10 Projection of earthquakes along profile OBS2012 in the Taiwan Shoal region. Velocity perturbation model is derived by subtracting the average one-dimensional velocity model from the final model. Inferred locations of faults are based on earthquake distribution.

In the Taiwan Shoal region, the earthquakes that have occurred at larger magnitudes than M_L4.0 exhibit a prominent southwest-to-northeast trend, which is similar to the trend of the strike of F1. It is also evident that the spatial distribution of the earthquake cluster coincides with the spatial extent and trend of F1 (Figs.1 and 2). Furthermore, the Taiwan Shoal region experienced 12 relatively great earthquakes with magnitudes of M_L5.0 to 6.0,

all of which were concentrated near F1.

We therefore conclude that earthquakes in the shallow outer rise occurred in the high-velocity area and were mainly controlled by the landward-dipping, southwest-northeast-striking, listric faults in the upper crust. Fig.10 depicts that most earthquakes occurred in the upper crust in the Taiwan Shoal region, although a few large normal earthquakes occurred in the lower crust. In general, the lower crust is plastic and the area is not prone to large earthquakes. However, a high velocity body exists in the lower crust in the Taiwan Shoal region, which results in lower crust embrittlement to some extent. Therefore, the lower crust accumulates stress and is capable of rupturing under the effect of the plate bending. Furthermore, the brittle lower crust is vulnerable to big faults extending from the upper crust to the lower crust. Therefore, some of these earthquakes occurred at the top of lower crust. It is also considered that blind faults are responsible for earthquakes occurring at deeper depths in the lower crust.

Previous studies found that aftershocks from the great September 1994 Taiwan Shoal earthquake were distributed over an area spanning approximately 40 km in an east-to-west direction, but that they mainly occurred in the western part of the area (Zheng *et al*., 1998). It is therefore more likely that the earthquakes occurring in the northwestern part of the Taiwan Shoal region were related to aftershocks rather than to seismic activity occurring along the southwest-northwest-striking normal faults. Many short fault segments that interact with each other are also developed in the Taiwan Shoal, and we therefore postulate that the sustained seismic activity in this region is also influenced by ubiquitous fault interactions through stress transfer, which is similar to that identified in the Koyna–Warna region of India (Gahalaut and Singh, 2004) and east of the city of Kerman in Iran (Nalbant *et al*., 2006; Walker *et al*., 2010).

However, the great September 1994 Taiwan Shoal earthquake does not appear to be related to the southwest-northeast-striking normal faults. The fault responsible for this earthquake exhibits a normal-faulting mechanism. The nodal planes indicate that they trend approximately east-to-west and that the horizontal maximum tensional stress axis runs from north to south (Kao and Wu, 1996; Zheng *et al*., 1998). In addition, the great September 1994 Taiwan Shoal earthquake occurred at a depth of 14 km (Zheng *et al*., 1998), which is deeper than most others in the region (Fig.10). We determined that the calculated epicenter of the earthquake (Zheng *et al*., 1998) was located close to the junction of F1 and F2 (Fig.11). F1 and F2 are representative of two different types of faults existing in the northeastern part of the SCS. F1-type faults strike southwest to northeast; they were accompanied by continental rifting during the Oligocene (*e.g.*, Taylor and Hayes, 1980; Ding *et al*., 2004, 2008) and remained active until the late Cenozoic in an extensional environment (Li *et al*., 2007). F2-type faults strike east-to-west and developed later that F1-type faults (during the early Cenozoic); their development was firstly curtailed by arc-continent collision in the Taiwan region and it then ceased entirely during the early Pleistocene (Zheng *et al*., 1998). Kirby *et al*. (1996). This indicates that preexisting faults that were previously active at shallow depths in the outer rise of the trench were later reactivated at greater depths. Studies focusing on these faults may thus be useful to assess seismic hazards within the region. On this evidence, we propose that the great September 1994 Taiwan Shoal earthquake was caused by reactivation of a preexisting fault (F2) which may have occurred in both the footwall and hanging wall.

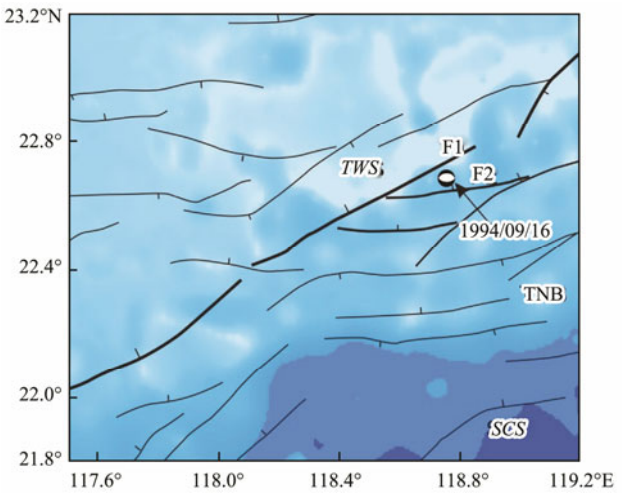

Fig.11 Distribution of faults in the northeastern SCS and epicenter location of September 16, 1994, earthquake. Faults were identified by interpretation of multichannel seismic data (Yang *et al*., 2015).

5.3 Potential Events in the Taiwan Shoal Region

Although outer-rise seismic activity is less common than interplate seismic activity, a global survey of outer-rise seismicity reveals a larger number of extensional events and fewer compressional events, for example in the Juan Fernandez Ridge off the Chilean coast (Fromm *et al*., 2006; Clouard *et al*., 2007), in the northern part of the Kermadec Trench north of New Zealand (Todd and Lay, 2013), and in the vicinity of Samoa (Lynnes and Lay, 1988; Lay *et al*., 2010) (Fig.12). Clouard *et al*. (2007) revealed that in-plane forces in the outer rise are directly related to subduction processes associated with stress accumulation and release during the seismic cycle. When subduction is locked, the outer-rise lithosphere is compressed (Astiz *et al*., 1988; Christensen and Ruff, 1988; Lay *et al*., 1989). However, when the crust slides, tension is present in the outer rise lithosphere because of slab pull (Kanamori, 1971; Abe, 1972). From a point in time five million years until recently, arc-continent collision proceeded along the Manila Trench (Huang *et al*., 2000) in the Taiwan Shoal region. Slab pull was resisted by the exposed precollision accretionary prism, and the resistive force caused in-plane compressive stress accumulation outside the Manila Trench. According to seismic records, there have been no further large extensional events (greater than M_L6.0) in the Taiwan Shoal regions since the September 1994 event indicating that a large drop in

stress occurred following the event. However, intermediate-magnitude earthquakes (M_L4.0–6.0) have occurred frequently in the past two decades since 1994 despite the absence of greater earthquakes. We therefore propose that a fault in this region may have accumulated a large slip deficit that has not been fully relieved by the September 1994 earthquake. This may explain that some of the relatively smaller earthquakes that have occurred frequently in such a short time interval within this fault. However, total stress is progressively accumulating within this fault, and it is only being slightly relieved by the small earthquakes. It is highly possible that accumulating stress will once again become too high, and we thus propose that another great earthquake may occur in the future in the Taiwan Shoal region.

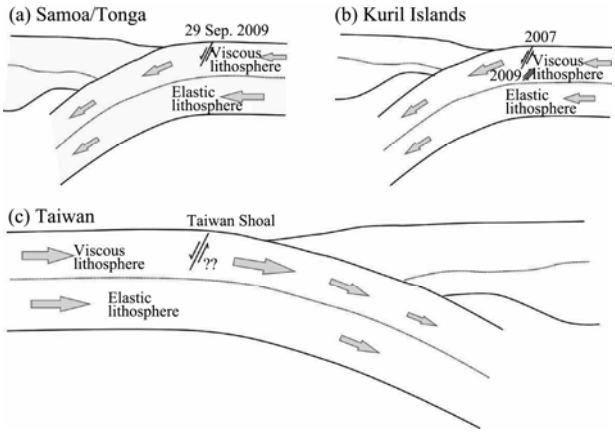

Fig.12 Schematic diagrams showing examples of earthquake patterns, including large, outer-rise normal-faulting and megathrust earthquakes. a) Great 2009 Samoa normal-faulting rupture beneath the outer rise (Lay *et al*., 2010); b) Great outer-rise normal-faulting earthquake and deeper megathrust earthquake occurring outside of trench (Lay *et al*., 2009); c) Possible location of great earthquake occurring on outer rise in Taiwan Shoal region (not with Manila Trench). Dashed lines represent boundary between viscous and elastic lithosphere, and arrows represent direction of subducted slab.

6 Conclusions

The crustal structure in the Taiwan Shoal region exhibits a heterogeneous velocity, which is manifested as high-velocity anomalies in the upper and lower crusts. Earthquakes at shallow depths have occurred in the Taiwan Shoal region outside of the Manila Trench. Our analyses suggest that the outer-rise earthquake cluster is located in the high-velocity upper crust in an area with strong asperities and a high stress concentration. Although no great earthquakes have occurred since the September 16, 1994, Taiwan Shoal earthquake, intermediate-magnitude (M_L 4.0–6.0) earthquakes have occurred frequently in this region. We propose that one fault accumulated a large slip deficit that was not fully relieved by the great 1994 event. Therefore, relatively small earthquakes have been occurring continuously since the event.

The September 16, 1994, earthquake and its aftershocks occurred independently of any seismic activity related to the northeast-to-southwest-striking listric faults that are located approximately parallel to the trench on the outer rise. Instead, the 1994 earthquake was an extensional faulting event that was most likely related to preexisting east-west-striking faults that were later reactivated. We suggest that the prominent earthquake cluster is influenced not only by the high-velocity anomaly in the upper crust but also by fault interactions. The Taiwan Shoal region exhibits a typical outer-rise crustal structure. Therefore, large intraslab earthquakes (such as those that occurring in the vicinity of Samoa and the northern Kermadec Trench) may also occur in this region in the future.

Acknowledgements

OBS data were obtained during a shared voyage with the Natural Science Foundation of China in 2012. Earthquake data were provided by the data centers of the China National Seismic Network (http://www.csndmc.ac.cn/newweb/index.jsp) and the Guangdong Seismic Network (http://www.gdsin.net/). The bathymetric chart was plotted using Generic Mapping Tools (Wessel and Smith, 1995) and the 2008 version of the General Bathymetric Chart of the Ocean (GEBCO_08, from 'The GEBCO_08 Grid, version 20090202', http://www.gebco.net). This work is supported by the Strategic Priority Research Program of Chinese Academy of Sciences (No. XDA13010101) and the National Natural Science Foundation of China (Nos. 91328206, 41676042, 41376060, and 41506046).

References

Abe, K., 1972. Lithospheric normal faulting beneath the Aleutian trench. *Physics of the Earth and Planetary Interiors*, **5**: 190-198.

Angelier, J., 1986. Geodynamics of the Eurasia-Phillippine Sea plate boundary: Perface. *Tectonophysics*, **125**: 9-10.

Astiz, L., Lay, T., and Kanamori, H., 1988. Large intermediate-depth earthquakes and the subduction process. *Physics of the Earth and Planetary Interiors*, **53** (1): 80-166.

Briais, A., Patriat, P., and Tapponnier, P., 1993. Updated interpretation of magnetic anomalies and seafloor spreading stages in the South China Sea: Implications for the Tertiary tectonics of Southeast Asia. *Journal of Geophysical Research*: *Solid Earth*, **98** (B4): 6299-6328.

Burchfiel, B., and Royden, L. H., 1985. North-south extension within the convergent Himalayan region. *Geology*, **13** (10): 679-682.

Chapple, W. M., and Forsyth, D. W., 1979. Earthquakes and bending of plates at trenches. *Journal of Geophysical Research: Solid Earth*, **84** (B12): 6729-6749.

Chen, C. H., Wang, W. H., and Teng, T. L., 2001. 3D velocity structure around the source area of the 1999 Chi-Chi, Taiwan, earthquake: Before and after the mainshock. *Bulletin Seismological Society of America*, **91** (5): 1013-1027.

Chen, C. X., Wu, S. G., and Zhao, C. L., 2014. Incoming plate variation along the north Manila Trench. In: *Subduction Dynamics: From Mantle Flow to Mega Disasters*. Morra, G., ed., John Wiley & Sons, Inc., Hoboken, New Jersey, 81-95.

Chen, E. M., and Huang, Y. Y., 1984. Nineteen strong earth-

quakes in South China–The summary of continental margin seismic belt along the northern South China Sea. *South China Journal of Seismology*, **4** (1): 11-32 (in Chinese with English abstract).

Cheng, W. B., 2004. Crustal structure of the high magnetic anomaly belt, western Taiwan, and its implications for continental margin deformation. *Marine Geophysical Researches*, **25** (1-2): 79-93.

Christensen, D. H., and Ruff, L. J., 1988. Seismic coupling and outer rise earthquakes. *Journal of Geophysical Research: Solid Earth*, **93** (B11): 13421-13444.

Clouard, V., Campos, J., Lemoine, A., Perez, A., and Kausel, E., 2007. Outer rise stress changes related to the subduction of the Juan Fernandez Ridge, central Chile. *Journal of Geophysical Research: Solid Earth*, **112** (B5): B05305.

Ding, W. W., Wang, Y. M., Chen, H. L., Yang, S. F., and Wu, N. Y., 2004. Deformation characters and its tectonic evolution of the Southwest Taiwan Basin. *Journal of Zhejiang University* (*Science Edition*), **31** (2): 216-220 (in Chinese with English abstract).

Ding, W. W., Li, J. B., Li, M. B., Qiu, X. L., Fang, Y. X., and Tang, Y., 2008. A Cenozoic tectono-sedimentary model of the Tainan Basin, the South China Sea: Evidence from a multichannel seismic profile. *Journal of Zhejiang University SCIENCE A*, **9** (5): 702-713.

Fromm, R., Alvarado, P., Beck, S., and Zandt, G., 2006. The April 9, 2001 Juan Fernández Ridge (M_w 6.7) tensional outer-rise earthquake and its aftershock sequence. *Journal of Seismology*, **10** (2): 163-170.

Gahalaut, V., and Singh, S., 2004. Fault interaction and earthquake triggering in the Koyna–Warna region, India. *Geophysical Research Letter*, **31** (11): L11614.

Guinness, E., Arvidson, R., Strebeck, J., Schulz, K., Davies, G., and Leff, C., 1982. Identification of a Precambrian rift through Missouri by digital image processing of geophysical and geological data. *Journal of Geophysical Research: Solid Earth*, **87** (B10): 8529-8545.

Hildenbrand, T. G., 1985. Rift structure of the northern Mississippi embayment from the analysis of gravity and magnetic data. *Journal of Geophysical Research: Solid Earth*, **90** (B14): 12607-12622.

Hildenbrand, T. G., Stuart, W., and Talwani, P., 2001. Geologic structures related to New Madrid earthquakes near Memphis, Tennessee, based on gravity and magnetic interpretations. *Engineering Geology*, **62** (1): 105-121.

Hinze, W. J., and Hildenbrand, T. G., 1988. The utility of geopotential field data in seismotectonic studies in the Eastern United States. *Seismological Research Letters*, **59** (4): 289-297.

Hsu, S. K., Yeh, Y. C., Doo, W. B., and Tsai, C. H., 2004. New bathymetry and magnetic lineations identifications in the northernmost South China Sea and their tectonic implications. *Marine Geophysical Researches*, **25** (1-2): 29-44.

Huang, C. Y., Xia, K., Yuan, P. B., and Chen, P. G., 2001. Structural evolution from Paleogene extension to Latest Miocene–Recent arc-continent collision offshore Taiwan: Comparison with on land geology. *Journal of Asian Earth Sciences*, **19** (5): 619-639.

Huang, C. Y., Yuan, P. B., Lin, C. W., Wang, T. K., and Chang, C. P., 2000. Geodynamic processes of Taiwan arc-continent collision and comparison with analogs in Timor, Papua New Guinea, Urals and Corsica. *Tectonophysics*, **325** (1): 1-21.

Kanamori, H., 1971. Seismological evidence for a lithospheric normal faulting–The Sanriku earthquake of 1933. *Physics of the Earth and Planetary Interiors*, **4** (4): 289-300.

Kao, H., and Wu, F. T., 1996. The 16 September 1994 earthquake (mb = 6.5) in the Taiwan strait and its tectonic implications. *Terrestrial Atmosphere and Oceanic Science*, **7** (1): 13-29.

Kao, H., Huang, G. C., and Liu, C. S., 2000. Transition from oblique subduction to collision in the northern Luzon arc-Taiwan region: Constraints from bathymetry and seismic observations. *Journal of Geophysical Research: Solid Earth*, **105** (B2): 3059-3079.

Kirby, S., Engdahl, R. E., and Denlinger, R., 1996. Intermediate-depth intraslab earthquakes and arc volcanism as physical expressions of crustal and uppermost mantle metamorphism in subducting slabs. In: *Subduction: Top to Bottom*. American Geophysical Union, 195-214.

Ku, C. Y., and Hsu, S. K., 2009. Crustal structure and deformation at the northern Manila Trench between Taiwan and Luzon Islands. *Tectonophysics*, **466** (3): 229-240.

Lay, T., Ammon, C. J., Kanamori, H., Rivera, L., Koper, K. D., and Hutko, A. R., 2010. The 2009 Samoa-Tonga great earthquake triggered doublet. *Nature*, **466** (7309): 964-968.

Lay, T., Astiz, L., Kanamori, H., and Christensen, D. H., 1989. Temporal variation of large intraplate earthquakes in coupled subduction zones. *Physics of the Earth and Planetary Interiors*, **54** (3-4): 258-312.

Lay, T., Kanamori, H., Ammon, C. J., Hutko, A. R., Furlong, K., and Rivera, L., 2009. The 2006–2007 Kuril Islands great earthquake sequence. *Journal of Geophysical Research: Solid Earth*, **114** (B11): B11308.

Lee, H. H., and Lin, J. Y., 2013. Seismic characteristics of outer-rise earthquakes in the different seismic coupling subduction zones. *Geophysical Research Abstracts*, **15**: EGU2013-4056.

Lees, J. M., and Malin, P. E., 1990. Tomographic images of P wave velocity variation at Parkfield, California. *Journal of Geophysical Research: Solid Earth*, **95** (B13): 21793-21804.

Lees, J. M., and Nicholson, C., 1993. Three-dimensional tomography of the 1992 southern California earthquake sequence: Constraints on dynamic earthquake rupture? *Geology*, **21** (5): 387-390.

Lester, R., Lavier, L. L., McIntosh, K., Van Avendonk, H. J., and Wu, F., 2012. Active extension in Taiwan's precollision zone: A new model of plate bending in continental crust. *Geology*, **40** (9): 831-834.

Lester, R., McIntosh, K., Van Avendonk, H. J., Lavier, L., Liu, C. S., and Wang, T., 2013. Crustal accretion in the Manila trench accretionary wedge at the transition from subduction to mountain-building in Taiwan. *Earth and Planetary Science Letters*, **375**: 430-440.

Lester, R., Van Avendonk, H. J., McIntosh, K., Lavier, L., Liu, C. S., Wang, T., and Wu, F., 2014. Rifting and magmatism in the northeastern South China Sea from wide-angle tomography and seismic reflection imaging. *Journal of Geophysical Research: Solid Earth*, **119** (3): 2305-2323.

Li, C. F., Zhou, Z., Hao, H., Chen, H., Wang, J., Chen, B., and Wu, J., 2008. Late Mesozoic tectonic structure and evolution along the present-day northeastern South China Sea continental margin. *Journal of Asian Earth Sciences*, **31** (4): 546-561.

Li, C. F., Zhou, Z., Li, J., Hao, H., and Geng, J., 2007. Structures of the northeasternmost South China Sea continental margin and ocean basin: Geophysical constraints and tectonic implications. *Marine Geophysical Researches*, **28** (1): 59-79.

Li, Y. X., Hu, X. K., Li, Z., Geng, H., Guo, L. Q., Guo, F. Y., and Liu, X. Y., 2002. Crustal movement and deformation in

Taiwan and its coastal area. *Acta Seismologica Sinica*, **15** (5): 510- 518.

Li, Z. X., and Li, X. H., 2007. Formation of the 1300-km-wide intracontinental orogen and postorogenic magmatic province in Mesozoic South China: A flat-slab subduction model. *Geology*, **35** (2): 179-182, DOI: 10.1130/G23193A.1.

Lin, A., Watts, A., and Hesselbo, S., 2003. Cenozoic stratigraphy and subsidence history of the South China Sea margin in the Taiwan region. *Basin Research*, **15** (4): 453-478, DOI: 10.1046/j.1365-2117.2003.00215.x.

Lin, S. J., Ding, X. R., Chen, W. W., and Chen, X. X., 2009. Research on focal mechanism solutions and tectonic stress field in Fujian region. *Journal of Geodesy and Geodynamics*, **29** (5): 27-32 (in Chinese with English abstract).

Liu, Y. X., Zhong, J. Q., and Zhan, W. H., 1994. The basic characteristics of seismic belts and preliminary analyses of regional stability in north continental margin of South China Sea. *South China Journal of Seismology*, **14** (4): 41-46 (in Chinese with English abstract).

Lynnes, C. S., and Lay, T., 1988. Source process of the great 1977 Sumba earthquake. *Journal of Geophysical Research: Solid Earth*, **93** (B11): 13407-13420.

Mishra, O., and Zhao, D., 2003. Crack density, saturation rate and porosity at the 2001 Bhuj, India, earthquake hypocenter: A fluid-driven earthquake? *Earth and Planetary Science Letters*, **212** (3): 393-405.

Müller, S., Choy, G. L., and Spence, W., 1996a. Inelastic models of lithospheric stress-I. Theory and application to outer-rise plate deformation. *Geophysical Journal International*, **125** (1): 39-53.

Müller, S., Spence, W., and Choy, G. L., 1996b. Inelastic models of lithospheric stress-II. Implications for outer-rise seismicity and dynamics. *Geophysical Journal International*, **125** (1): 54-72.

Nalbant, S. S., Steacy, S., and McCloskey, J., 2006. Stress transfer relations among the earthquakes that occurred in Kerman province, southern Iran since 1981. *Geophysical Journal International*, **167** (1): 309-318.

Ren, Z. Y., Luo, Z. N., and Hua, W., 2002. Characteristics of the seismicity and analysis of earthquake situation in the border area of Guangdong, Fujian and Jiangxi. *South China Journal of Seismology*, **22** (3): 28-38 (in Chinese with English abstract).

Saada, S. A., 1983. *Elasticity: Theory and Applications*. Pergamon Press, New York, 395-428.

Seno, T., 1993. A model for the motion of the Philippine Sea Plate consistent with NUVEL-1 and geological data. *Journal of Geophysical Research: Solid Earth*, **98** (B10): 17941-17948.

Seno, T., and Yamanaka, Y., 1996. Double seismic zones, compressional deep trench-outer rise events, and superplumes. *Subduction: Top to Bottom*: 347-355.

Shi, H., and Li, C. F., 2012. Mesozoic and early Cenozoic tectonic convergence-to-rifting transition prior to opening of the South China Sea. *International Geology Review*, **54** (15): 1801-1828, DOI: 10.1080/00206814.2012.677136.

Sibuet, J., and Hsu, S. K., 2004. How was Taiwan created. *Tectonophysics*, **379**: 159-181.

Sibuet, J. C., Hsu, S. K., and Debayle, E., 2004. Geodynamic context of the Taiwan orogen. In: *Continent-Ocean Interactions Within East Asian Marginal Seas*. Clift, P. D., *et al*., eds., Geophysics Monogr Series, AGU, Washington, 127-158.

Simons, W., Socquet, A., Vigny, C., Ambrosius, B., Haji Abu, S., Promthong, C., Subarya, C., Sarsito, D., Matheussen, S., and Morgan, P., 2007. A decade of GPS in southeast Asia: Resolving Sundaland motion and boundaries. *Journal of Geophysical Research: Solid Earth*, **112** (B6): B06420.

Srinagesh, D., Singh, S., Reddy, K. S., Prakasam, K., and Rai, S., 2000. Evidence for high velocity in Koyna seismic zone from P-wave teleseismic imaging. *Geophysical Research Letters*, **27** (17): 2737-2740.

Stauder, W., 1968a. Mechanism of the Rat Island earthquake sequence of February 4, 1965, with relation to island arcs and sea-floor spreading. *Journal of Geophysical Research*, **73** (12): 3847-3858.

Stauder, W., 1968b. Tensional character of earthquake foci beneath the Aleutian Trench with relation to sea-floor spreading. *Journal of Geophysical Research*, **73** (24): 7693-7701.

Sun, J. L., Xu, H. L., Zhan, W. H., and Cao, J. H., 2012. Activity and triggering mechanism of seismic belt along the northern South China Sea continental margin. *Journal of Tropical Oceanography*, **31** (3): 40-47 (in Chinese with English abstract).

Taylor, B., and Hayes, D. E., 1980. The tectonic evolution of the South China Basin. *Geophysical Monograph Series: The Tectonic and Geologic Evolution of Southeast Asian Seas and Islands*, **23**: 89-104.

Taylor, B., and Hayes, D. E., 1983. Origin and history of the South China Sea Basin. *Geophysical Monograph Series: The Tectonic and Geologic Evolution of Southeast Asian Seas and Islands*, **27**: 23-56.

Todd, E. K., and Lay, T., 2013. The 2011 northern Kermadec earthquake doublet and subduction zone faulting interactions. *Journal of Geophysical Research: Solid Earth*, **118** (1): 249-261.

Turcotte, D. L., and Schubert, D., 2001. *Geodynamics.* 2nd edition. Cambridge University, New York, 213pp.

Walker, R. T., Talebian, M., Saiffori, S., Sloan, R. A., Rasheedi, A., MacBean, N., and Ghassemi, A., 2010. Active faulting, earthquakes, and restraining bend development near Kerman city in southeastern Iran. *Journal of Structural Geology*, **32** (8): 1046-1060.

Wan, K. Y., Cao, J. H., Xia, S. H., Sun, J. L., Huang, H. B., and Xu, H. L., 2016. Characteristics of secondary Pg phases from OBS wide-angle seismic survey and their role in crustal imaging. *Chinese Journal of Geophysics–Chinese Edition*, **59** (4): 427-441.

Wan, K. Y., Xia, S. H., Cao, J. H., Sun, J. L., and Xu, H. L., 2017. Deep seismic structure of the northeastern South China Sea: Origin of a high-velocity layer in the lower crust. *Journal of Geophysical Research: Solid Earth*, **122** (4): 2831-2858, DOI: 10.1002/2016JB013481.

Wang, D., and Shu, L., 2012. Late Mesozoic basin and range tectonics and related magmatism in southeast China. *Geoscience Frontiers*, **3** (2): 109-124.

Wang, T. K., Chen, M. K., Lee, C. S., and Xia, K., 2006. Seismic imaging of the transitional crust across the northeastern margin of the South China Sea. *Tectonophysics*, **412** (3): 237-254.

Wang, Z., and Zhao, D., 2006. Seismic images of the source area of the 2004 mid-Niigata prefecture earthquake in northeast Japan. *Earth and Planetary Science Letters*, **244** (1): 16-31.

Wang, Z., Su, J., Liu, C., and Cai, X., 2015. New insights into the generation of the 2013 Lushan earthquake (Ms 7.0), China. *Journal of Geophysical Research: Solid Earth*, **120** (5): 3507-3526.

Woolard, G. P., 1959. Crustal structure from gravity and seismic measurements. *Journal of Geophysical Research*, **64**: 1521-

1544.

Wu, W. N., Hsu, S. K., Lo, C. L., Chen, H. W., and Ma, K. F., 2009. Plate convergence at the westernmost Philippine Sea Plate. *Tectonophysics*, **466** (3): 162-169.

Xia, K. Y., Huang, C. L., Jiang, S. R., Zhang, Y. X., Su, D. Q., Xia, S. G., and Chen, Z. R., 1994. Comparison of the tectonics and geophysics of the major structural belts between the northern and southern continental margins of the South China Sea. *Tectonophysics*, **235** (1): 99-116.

Xia, S., Zhao, D., and Qiu, X., 2008. The 2007 Niigata earthquake: Effect of arc magma and fluids. *Physics of the Earth and Planetary Interiors*, **166** (3): 153-166.

Xu, H. L., Qiu, X. L., Zhao, M. H., Sun, J. L., and Zhu, J. J., 2006. Characteristics of the crustal structure and hypocentral tectonics in the epicentral area of Nan'ao earthquake (M7.5), the northeastern South China Sea. *Chinese Science Bulletin*, **51** (S2): 83-91 (in Chinese with English abstract).

Yan, Q., Shi, X., and Castillo, P. R., 2014. The late Mesozoic–Cenozoic tectonic evolution of the South China Sea: A petrologic perspective. *Journal of Asian Earth Sciences*, **85**: 178-201.

Yang, S. X., Qiu, Y., and Zhu, B. D., 2015. *Atlas of Geology and Geophysics of the South China Sea*. China Navigation Publications, Tianjin.

Zelt, C., and Smith, R., 1992. Seismic traveltime inversion for 2-D crustal velocity struct*ure. Geophysical Journal International*, **108** (1): 16-34.

Zhang, P. Z., Wang, Q., and Ma, Z. J., 2002. GPS velocity field and active crustal blocks of contemporary tectonic deformation in continental China. *Earth Science Frontiers*, **9** (2): 431-441 (in Chinese with English abstract).

Zhang, J. H., Li, Y. X., and Guo, L. Q., 2005. Contemporary tectonic movement and internal deformation of South China block. *Journal of Geodesy and Geodynamics*, **25** (3): 59-62 (in Chinese with English abstract).

Zhang, P. Z., Wang, Q., and Ma, Z. J., 2002. GPS velocity field and active crustal deformation and around Qinghai Tibet plateau. *Earth Science Frontiers*, **9** (2): 442-450 (in Chinese with English abstract).

Zhao, D., Hasegawa, A., and Horiuchi, S., 1992. Tomographic imaging of P and S wave velocity structure beneath northeastern Japan. *Journal of Geophysical Research: Solid Earth*, **97** (B13): 19909-19928, DOI: 10.1029/92 JB00603.

Zhao, D., Kanamori, H., Negishi, H., and Wiens, D., 1996. Tomography of the source area of the 1995 Kobe earthquake: Evidence for fluids at the hypocenter? *Science*, **274** (5294): 1891-1894.

Zhao, D., Mishra, O., and Sanda, R., 2002. Influence of fluids and magma on earthquakes: Seismological evidence. *PEPI*, **132** (4): 249-267.

Zhao, D., Tani, H., and Mishra, O., 2004. Crustal heterogeneity in the 2000 western Tottori earthquake region: Effect of fluids from slab dehydration. *Physics of the Earth and Planetary Interiors*, **145** (1): 161-177.

Zheng, T. Y., Ai, Y. S., and Chen, Q. Z., 1998. The 16 September 1994 Taiwan Strait earthquake: A simple rupture event starting as a break of asperity. *Physics of the Earth and Planetary Interiors*, **107** (4): 269-284.

Zhou, D., Wang, W., Wang, J., Pang, X., Cai, D., and Sun, Z., 2006. Mesozoic subduction-accretion zone in northeastern South China Sea inferred from geophysical interpretations. *Science in China Series D*, **49** (5): 471-482.

Zhou, S. Y., Shu, A. P., and Zhang, Y. G., 2000. Present-day crustal movement in China continent and its southeast coast region. *Progress in Natural Science*, **10** (7): 536-541 (in Chinese with English abstract).

Zhou, X., and Li, W., 2000. Origin of late Mesozoic igneous rocks in southeastern China: Implications for lithosphere subduction and underplating of mafic magmas. *Tectonophysics*, **326** (3): 269-287.

(Edited by Chen Wenwen)